Surface & Coatings Technology 231 (2013) 19–23

Contents lists available at ScienceDirect

Surface & Coatings Technology

journal homepage: www.elsevier.com/locate/surfcoat

Characterization of W–Ta–N hard films synthesized by direct current magnetron sputtering

J.F. Yang [a,b], Z.G. Yuan [a], X.P. Wang [a], Q.F. Fang [a,*]

[a] Key Laboratory of Materials Physics, Institute of Solid State Physics, Chinese Academy of Sciences, Hefei 230031, People's Republic of China
[b] Department of Applied Physics and Mechanical Engineering, Lulea University of Technology, SE-971 87 Luleå, Sweden

ARTICLE INFO

Available online 6 July 2012

Keywords:
Hard films
Magnetron sputtering
AFM
Hardness
Adhesion strength

ABSTRACT

W–Ta–N hard films with Ta/(W+Ta) = 46 at.% were deposited on single crystal Si (111) substrates using direct current magnetron sputtering. The effect of nitrogen partial pressure (p_{N2}) on crystal structure, surface topography, adhesion strength, and hardness of W–Ta–N films was investigated. With increasing p_{N2}, the phase composition changes from pure fcc W–Ta–N phase to a mixture of fcc W–Ta–N phase and hexagonal δ-W(Ta)N phase, and then to pure hexagonal δ-W(Ta)N phase; the average grain size decreases monotonously; the surface becomes more and more smooth; the hardness initially increases and then decreases after passing a maximum of 41 GPa at p_{N2} = 0.5 Pa, while the adhesion strength varies in an opposite trend to the hardness. The maximum hardness could be due to the combined effect of reduced crystallite size and the coexistence of two phases.

© 2012 Elsevier B.V. All rights reserved.

1. Introduction

Deposition of transition metal nitride and carbide thin films on the surface of tools can greatly improve the cutting performance and extend the lifetime of these tools [1–3]. To date, titanium nitride or chromium nitride based films have been thoroughly studied and used successfully in industrial field [4–6]. Especially, superhard Ti–Si–N coatings with hardness of up to 50 GPa, and thermal stability of up to 800 °C have attracted great interest [7].

Tungsten nitride films have attracted more and more attention for mechanical applications since 1994 [8]. To meet ever increasing requirement for superior comprehensive properties, the addition of the third element to form ternary nitride coatings by co-sputtering was investigated such as W–Ti–N [9], W–Si–N [10], W–Ge–N [11], and W–Cr–N [12]. The structure and properties of ternary nitride coatings strongly depend on the properties and concentration of the third element. Louro et al. [13] reported that there is a preferential bonding order from Si–N through Si–W to W–N bonds in W–Si–N coatings under different nitrogen partial pressures due to the different formation heat that decreases sequentially from Si–N, Si–W to W–N. It is known that the formation heat between tantalum and nitrogen is much lower than that between tungsten and nitrogen [14]. Therefore, it is expected that tantalum could play the same important role in adjusting the structure of W–Ta–N coatings as silicon in the W–Si–N coatings. In this study, W–Ta–N films with Ta/(W+Ta) = 46 at.% were fabricated using dc magnetron sputtering with nitrogen partial pressure in the range of 0.07–0.63 Pa. The influence of nitrogen partial pressure on W–Ta–N films was investigated systematically in terms of the average crystallite sizes, preferred orientation, surface topography, hardness, and adhesion strength.

2. Experimental procedure

W–Ta–N films were fabricated by reactive direct current (dc) sputtering technique from a W–Ta mosaic target (purity of 99.5%) that was prepared by attaching a tantalum sheet to a circular (ϕ60 mm × 2 mm) tungsten plate. Silicon (111) wafer was used as substrate. All substrates were ultrasonically cleaned using a mixture of acetone and alcohol, rinsed in deionized water, dried in a nitrogen jet, and then immediately introduced into the vacuum chamber. The substrate was fixed to the tilted substrate holder with a distance of about 55 mm away from the target. The substrate was electrically grounded.

The vacuum chamber was pumped down to 8×10^{-4} Pa at first and then the substrate was heated up to 450 °C. High-purity argon was introduced into the chamber through a mass flow controller (MFC) and a 20 min pre-sputtering was carried out to clean the target surface. The dc power and work pressure for the pre-sputtering were kept at about 120 W and 2 Pa, respectively. After pre-sputtering, nitrogen was introduced into the chamber through a MFC. The total working pressure and dc power during sputtering of the W–Ta–N films were kept constant at 0.7 Pa and 100 W, respectively.

Phase composition and crystalline structure of the films were analyzed with grazing incidence X-ray diffraction (Philips X'pert PRO MPD) in the scanning range from 30° to 90° stepped by 0.06°, using monochromatized Cu Kα radiation operating at 40 kV and 40 mA. The cell parameter of deposited films was evaluated by the whole pattern refinement of XRD patterns using the Fullprof program [15].

* Corresponding author. Tel.: +86 551 559 1459; fax: +86 551 559 1434.
E-mail address: qffang@issp.ac.cn (Q.F. Fang).

0257-8972/$ – see front matter © 2012 Elsevier B.V. All rights reserved.
doi:10.1016/j.surfcoat.2012.06.082

Surface topography and roughness were characterized by AFM (Veeco AutoProbe CP) in contact mode at atmosphere condition. Cross-section morphology of coatings was characterized with a field-emission scanning electron microscope (FESEM, Sirion 200, FEI). The elemental composition of W–Ta–N films was determined by energy dispersive spectroscopy (EDS) equipped in FESEM. The thickness of all films was determined by measuring the cross-section of the as deposited films with FESEM and the deposition rate was calculated from the total thickness divided by the deposition time.

The microhardness and Young's modulus of the films were measured with a nanoindentation apparatus (MTS NANO Indenter® G200) at room temperature. In the hardness measurements, the penetration depth was kept at about 1/7–1/10 of the film thickness to avoid the effects of substrate and the surface roughness of films. The data of hardness was averaged from 9 indentation tests for each sample to improve measurement accuracy, and the measurements were calibrated with reference sample of fused quartz with hardness of 10 GPa.

The adhesion strength of a film/substrate system is normally defined as the energy needed to separate the film from the substrate. Since it is difficult to measure this kind of energy, the maximum force needed to separate the film from the substrate is instead considered as the indicator of the adhesion strength. Generally, in the scratch test, the critical load, L_C, at which failure occurs, is used to evaluate the adhesion strength of the film/substrate system. In this work, the adhesion strength between film and substrate was evaluated with a scratch tester (WS-2005 equipped with an acoustic emission (AE) detector) by increasing load from 0 to 100 N at a loading rate of 50 N/min. The standard diamond Rockwell C indenter tip of 200 μm in radius was used during scratch. The scratch length and the scratch rate were fixed as 10 mm and 5 mm/min, respectively.

3. Results and discussion

3.1. Elemental composition

Fig. 1 displays the elemental composition of W–Ta–N films under different nitrogen partial pressures. With nitrogen partial pressure increasing from 0.07 to 0.28 Pa the N concentration in W–Ta–N films increases gradually from 20 to 45 at.%, in contrast, the Ta and W concentrations decrease from 36.8 to 26.3 at.% and from 43.2 to 29.7 at.%, respectively. With further increase of nitrogen partial pressure, the nitrogen concentration increases slowly and reaches a saturated value of approximately 50 at.%, correspondingly, the W and Ta concentrations decrease slowly at first and then kept nearly unchanged. The overall atomic ratio of Ta/(W + Ta) keeps a nearly constant value of approximately 46 at.%, regardless of p_{N2}. Table 1 presents the deposition rate and thickness of W–Ta–N coatings. The deposition rate of W–Ta–N films decreased from 0.59 to 0.49 nm/s as the nitrogen

Table 1
Deposition rate and thickness of W–Ta–N coatings deposited on silicon substrate under different nitrogen partial pressures.

Nitrogen partial pressure (Pa)	Deposition rate (nm/s)	Thickness (μm)
0.07	0.59	2.2
0.18	0.56	2.2
0.28	0.50	2.1
0.4	0.49	2.1
0.5	0.47	2.1
0.63	0.46	2.2

partial pressure increased from 0.07 to 0.4 Pa, but changed slightly with further increase of nitrogen partial pressure. In our experiments, the working pressure maintained unchanged, therefore with the increase of nitrogen partial pressure, the argon partial pressure decreased. Subsequently, the decrease in the number of Ar^+ ion that bombarded target led to less W and Ta sputtering, and thus the deposition rate of W–Ta–N coatings decreased.

3.2. Structure

XRD patterns of W–Ta–N films deposited at different nitrogen partial pressures were presented in Fig. 2. When the nitrogen partial pressure is in the range of 0.07–0.40 Pa, the films exhibit face centered cubic (fcc) NaCl type structure as indicated by the occurrence of (111), (200), (220), (311), and (222) diffraction peaks. At p_{N2} = 0.50 Pa, a new diffraction peak was detected at the left side of the (111) diffraction peak of the fcc phase, which can be ascribed to the (100) plane of the hexagonal phase, δ-W(Ta)N. This illustrates that the film exhibits a mixture of fcc W–Ta–N phase and hexagonal δ-W(Ta)N phase. For W–Ta–N films deposited at p_{N2} = 0.63 Pa, only the hexagonal δ-W(Ta)N phase was detected, as indicated by the diffraction lines from the (100), (110), and (200) planes. This illustrates that the phase composition of the W–Ta–N films changes from pure fcc W–Ta–N phase to a mixture of fcc W–Ta–N phase and hexagonal δ-W(Ta)N phase and then to pure hexagonal δ-W(Ta)N phase when the nitrogen fraction changes from 0.07 to 0.63 Pa in a total working pressure of 0.7 Pa, as shown in Fig. 3. The evolution of crystalline structure of W–Ta–N coatings from fcc to hexagonal with increasing nitrogen partial pressure can be understood from the point of view of thermodynamics: in fcc W_2N structure W atoms occupy the positions of the fcc lattice points and N atoms occupy 50% of the total octahedral sites. As nitrogen partial pressure was increased, the excessive nitrogen atom will occupy other vacant octahedral sites, and led to increase in lattice distortion. Therefore, the strain energy in coatings increased with

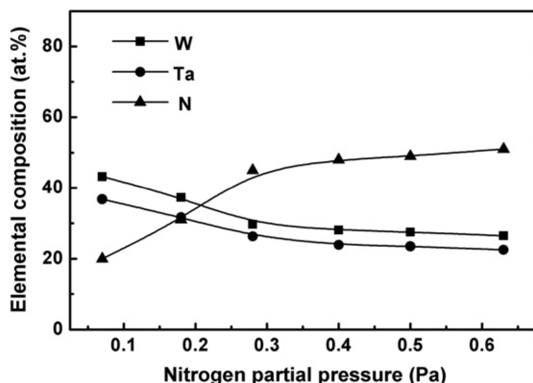

Fig. 1. Elemental composition of W–Ta–N films deposited at different nitrogen partial pressures.

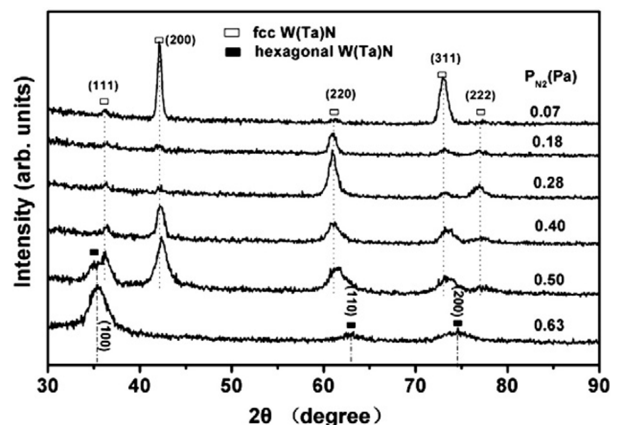

Fig. 2. XRD patterns of W–Ta–N films deposited at different nitrogen partial pressures.

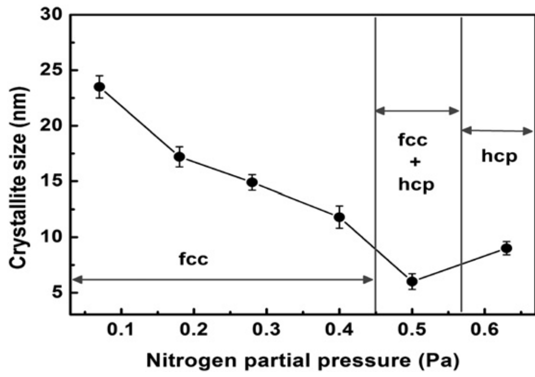

Fig. 3. Nitrogen partial pressure dependence of average crystallite size of W–Ta–N films and a simple phase diagram.

nitrogen partial pressure, as it is beyond certain threshold value, the crystalline structure changes from fcc to hexagonal in order to minimize the overall energy.

As observed from Fig. 2, although all the films deposited at nitrogen partial pressure in the range of 0.07–0.40 Pa show fcc structure, the width and relative intensity of diffraction peaks varied noticeably with increasing nitrogen partial pressure, indicating the change of crystallite size. In order to clarify these phenomena more explicitly, the average crystallite size in W–Ta–N films were calculated according to Debye–Scherrer equation. Fig. 3 shows the average crystallite size in W–Ta–N films at different nitrogen partial pressures, where a simple phase diagram was also shown. At $p_{N2} = 0.07$ Pa, the crystallite size is approximately 24 nm. With the increase of nitrogen partial pressure the crystallite size monotonously decreases and reaches the minimum of about 6 nm at $p_{N2} = 0.50$ Pa, and then increases slightly with further increase in nitrogen partial pressure. The grain size exhibited an overall decrease trend with increasing nitrogen partial pressure. It is known that the grain growth is characterized by nucleation and subsequent adsorption of other atoms. As the nitrogen partial pressure was increased, more nitrogen atoms were deposited onto the surface of substrate, which block other tantalum or tungsten atoms to move towards the existing nucleation, and thus reduce the grain size. It is interesting to note that the smallest average grain size appears in the zone of mixed phases, which is reasonable since the coexistence of multiple phases may lead to smaller average grain size, as reported in literature [16]. In addition, it can be observed that with increasing nitrogen partial pressure the diffraction peaks shifted slightly to higher diffraction angles, indicating the decrease in lattice constant. In fact, the lattice constant of fcc W–Ta–N coatings is 4.123, 4.120. 4.115, 4.112 and 4.110 Å, when the nitrogen partial pressure is 0.07, 0.18, 0.28, 0.40 and 0.50, respectively.

3.3. Surface topography and cross section morphology

Fig. 4 displays the surface topographies and root mean square roughness (RMSR) of W–Ta–N films deposited under different nitrogen partial pressures. All the films show a granular morphology. At $p_{N2} = 0.07$ Pa, the film shows a relatively rough surface with a RMSR of 40 nm as seen in Fig. 4a and f. In Fig. 4b ($p_{N2} = 0.28$ Pa), smaller crystallites are formed but the size difference between the largest and smallest crystallites is still obvious. At higher N_2 partial pressure of

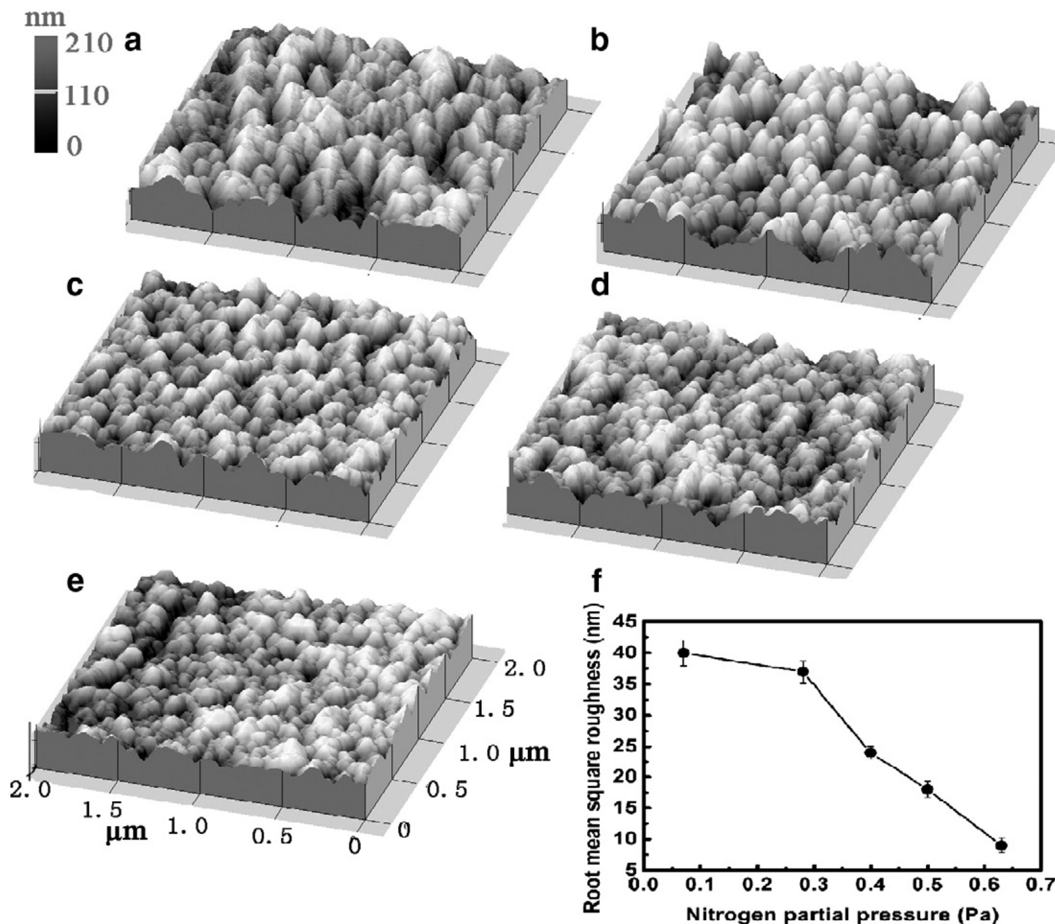

Fig. 4. AFM surface topography of W–Ta–N films under different nitrogen partial pressures: (a) 0.07 Pa, (b) 0.28 Pa, (c) 0.40 Pa, (d) 0.50 Pa, and (e) 0.63 Pa; panel f is the variation of root mean square roughness of W–Ta–N films under different nitrogen partial pressures.

p_{N2} = 0.40, 0.50, and 0.63 Pa (Fig. 4c, d, and e), the average crystallite size decreases dramatically. Correspondingly, the RMSR decreases from 24 nm at p_{N2} = 0.40 Pa to 18 nm at p_{N2} = 0.50 Pa, and then to 9 nm at p_{N2} = 0.63 Pa as exhibited in Fig. 4f.

The effect of nitrogen partial pressure on the cross-sectional morphology of W–Ta–N films is shown in Fig. 5. When p_{N2} = 0.07 and 0.28 Pa the W–Ta–N films show a typical columnar structure (Fig. 5a and b) with a few cavity and porosity distributed around the columnar grain boundary. When p_{N2} = 0.40 Pa or higher, the W–Ta–N films exhibit a densely compacted structure (Fig. 5c).

3.4. Hardness and Young's modulus

Fig. 6 shows the evolution of hardness and Young's modulus of W–Ta–N films with nitrogen partial pressure. At p_{N2} = 0.07 Pa, the hardness and Young's modulus of the W–Ta–N films are 23 GPa and 280 GPa, respectively. As the nitrogen partial pressure increases to 0.18, 0.28, 0.40, and 0.5 Pa, the hardness and Young's modulus of the W–Ta–N films increase to 27, 33, 36, and 41 GPa and to 300, 310, 340, and 390 GPa, respectively, reaching their maximum value at p_{N2} = 0.50 Pa. At p_{N2} = 0.63 Pa, the hardness and Young's modulus of the W–Ta–N films decrease to 38 GPa and 360 GPa, respectively. Since the evolution of hardness with nitrogen partial pressure shows the nearly opposite trend as the crystallite size, the hardness enhancement can be reasonably ascribed dominantly to the strengthening effect of grain size refinement. In addition, the nanocomposite structure comprising a mixture of fcc W–Ta–N and hexagonal W(Ta)N phases would be another possible factor for the highest hardness of the film deposited at pN2 = 0.5 Pa.

3.5. Adhesion strength

Fig. 7 shows the variation of elastic recovery of W–Ta–N films and adhesion strength between W–Ta–N films and silicon substrate with the nitrogen partial pressure. In contrast to the hardness and Young's modulus, the adhesion strength of W–Ta–N films decreases from 49 N to 25 N at first and then increases to 28 N, indicating that the film with higher hardness has relatively poor adhesion strength, which can be understood by the variation of the toughness of films. As it is well known, the toughness of films can be expressed qualitatively by the elastic recovery (We), defined as the ratio of the recovery displacement after unloading to the total indentation displacement [17]. In general, higher elastic recovery represents lower toughness. The elastic recovery of W–Ta–N films calculated from the corresponding load–displacement curves (not shown here) are 27%, 31%, 32%, 35%, 43%, and 41% at p_{N2} = 0.07, 0.18, 0.28, 0.40, 0.50, and 0.63 Pa, respectively, corresponding to the hardness of 23, 27, 33, 36, 41, and 38 GPa. This indicates that the higher the hardness is, the more brittle the W–Ta–N films are. Thus, the decrease of adhesion strength with increasing hardness can be understood by the decrease of the toughness of W–Ta–N films.

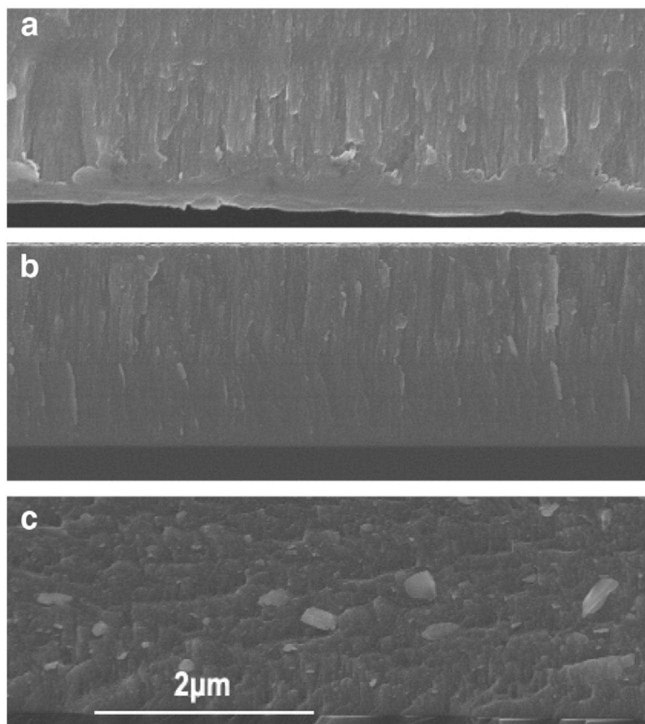

Fig. 5. Cross-section morphology of W–Ta–N films under different nitrogen partial pressures: (a) 0.07 Pa, (b) 0.28 Pa, and (c) 0.40 Pa.

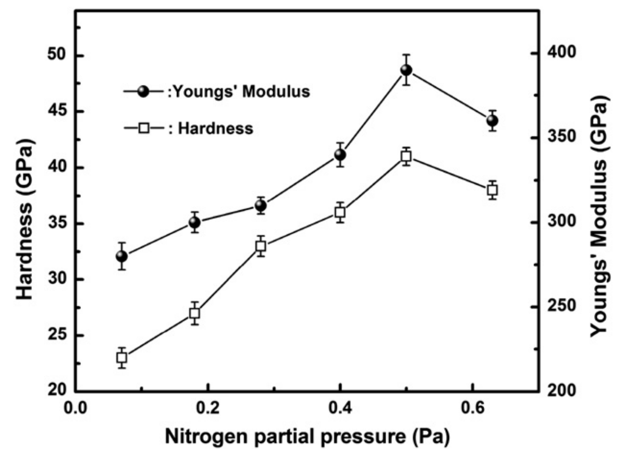

Fig. 6. Variation of the hardness and Young's modulus of W–Ta–N films with nitrogen partial pressure.

4. Conclusions

W–Ta–N films were synthesized using reactive dc magnetron sputtering and the influence of nitrogen partial pressure on crystalline structure, surface topography, adhesion strength, and hardness of the W–Ta–N films was investigated.

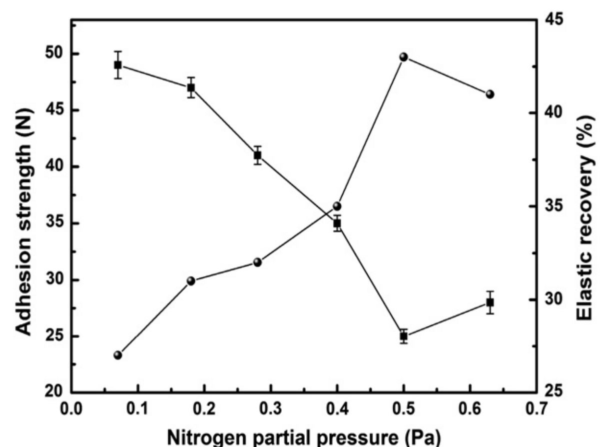

Fig. 7. Elastic recovery and adhesion strength between W–Ta–N coatings and silicon substrate as a function of nitrogen partial pressure.

As nitrogen partial pressure increases from 0.07 to 0.63 Pa in a total working pressure of 0.7 Pa, the structure of the films changes from pure fcc W – Ta – N phase to a mixture of fcc W – Ta – N phase and hexagonal δ-W(Ta)N phase and then to pure hexagonal δ-W(Ta)N phase, the crystallite size of the fcc W – Ta – N phase decreases gradually, and reaches to the minimum value of about 6 nm at $p_{N2} = 0.50$ Pa. With the increasing nitrogen partial pressure, the hardness initially increases and then decreases after passing a maximum of 41 GPa at $p_{N2} = 0.5$ Pa, while the adhesion strength varies in an opposite trend to the hardness. The maximum hardness could be due to the combined effect of reduced crystallite size and mixture of two phases.

Acknowledgments

This work has been subsidized by the National Natural Science Foundation of China (Grant No. 51101152). The first author thanks the Swedish Institute scholarship for the support of his research work at Lulea University of Technology, Sweden.

References

[1] G. Keller, I. Barzen, R. Erz, Fresenius J. Anal. Chem. 341 (1991) 349.
[2] A. Cavaleiro, M.T. Vieira, G. Lemperiere, Thin Solid Films 197 (1–2) (1991) 237.
[3] R.A. Andrievski, J. Mater. Sci. 32 (1997) 4463.
[4] C. Rebholz, H. Ziegele, A. Leyland, Surf. Coat. Technol. 115 (1999) 222.
[5] S. Zhang, Y.Q. Fu, H.J. Du, X.T. Zeng, Surf. Coat. Technol. 162 (2003) 42.
[6] I. Efeoglu, R.D. Arnell, S.F. Tinston, D.G. Teer, Surf. Coat. Technol. 57 (1993) 117.
[7] S. Veprek, M.G.J. Veprek-Heijman, P. Karvankova, Thin Solid Films 476 (2005) 1.
[8] J. Castanho, A. Cavaleiro, M.T. Vieira, Vacuum 45 (1994) 1051.
[9] A. Cavaleiro, B. Trindade, M.T. Vieira, Surf. Coat. Technol. 174–175 (2003) 68.
[10] C. Louro, A. Cavaleiro, Surf. Coat. Technol. 116–119 (1999) 74.
[11] A.P. Piedadea, M.J. Gomes, J.F. Pierson, A. Cavaleiro, Surf. Coat. Technol. 200 (2006) 6303.
[12] B.S. Yau, C.W. Chu, D. Lin, Thin Solid Films 516 (2008) 1877.
[13] C. Louro, A. Cavaleiro, F. Montemor, Surf. Coat. Technol. 142–144 (2001) 964.
[14] G.V. Samsonov, I.M. Vinitskii, In: Handbook of Refractory Compounds, IFI/Plenum, New York, 1980, p. 129.
[15] J. Rodriguez-Carvajal, Physica B 192 (1993) 55.
[16] P. Hones, N. Martin, M. Regula, F. Lévy, J. Phys. D: Appl. Phys. 36 (2003) 1023.
[17] W.T. Zheng, H. Sjostrom, I. Ivanov, J. Vac. Sci. Technol. A 14 (1996) 2696.